SiC Composite for Fuel Structure Applications

DOE-EPRI-0000539

Final Report, December 22, 2017

DISCLAIMER OF WARRANTIES AND LIMITATION OF LIABILITIES

THIS DOCUMENT WAS PREPARED BY THE ORGANIZATION(S) NAMED BELOW AS AN ACCOUNT OF WORK SPONSORED OR COSPONSORED BY THE ELECTRIC POWER RESEARCH INSTITUTE, INC. (EPRI). NEITHER EPRI, ANY MEMBER OF EPRI, ANY COSPONSOR, THE ORGANIZATION(S) BELOW, NOR ANY PERSON ACTING ON BEHALF OF ANY OF THEM:

(A) MAKES ANY WARRANTY OR REPRESENTATION WHATSOEVER, EXPRESS OR IMPLIED, (I) WITH RESPECT TO THE USE OF ANY INFORMATION, APPARATUS, METHOD, PROCESS, OR SIMILAR ITEM DISCLOSED IN THIS DOCUMENT, INCLUDING MERCHANTABILITY AND FITNESS FOR A PARTICULAR PURPOSE, OR (II) THAT SUCH USE DOES NOT INFRINGE ON OR INTERFERE WITH PRIVATELY OWNED RIGHTS, INCLUDING ANY PARTY'S INTELLECTUAL PROPERTY, OR (III) THAT THIS DOCUMENT IS SUITABLE TO ANY PARTICULAR USER'S CIRCUMSTANCE; OR

(B) ASSUMES RESPONSIBILITY FOR ANY DAMAGES OR OTHER LIABILITY WHATSOEVER (INCLUDING ANY CONSEQUENTIAL DAMAGES, EVEN IF EPRI OR ANY EPRI REPRESENTATIVE HAS BEEN ADVISED OF THE POSSIBILITY OF SUCH DAMAGES) RESULTING FROM YOUR SELECTION OR USE OF THIS DOCUMENT OR ANY INFORMATION, APPARATUS, METHOD, PROCESS, OR SIMILAR ITEM DISCLOSED IN THIS DOCUMENT.

REFERENCE HEREIN TO ANY SPECIFIC COMMERCIAL PRODUCT, PROCESS, OR SERVICE BY ITS TRADE NAME, TRADEMARK, MANUFACTURER, OR OTHERWISE, DOES NOT NECESSARILY CONSTITUTE OR IMPLY ITS ENDORSEMENT, RECOMMENDATION, OR FAVORING BY EPRI.

THE ELECTRIC POWER RESEARCH INSTITUTE (EPRI) PREPARED THIS REPORT.

This work was generated with the financial support from the US. Government through Contract/Award number NE0000539, and as such the U.S. Government retains a paid-up non-exclusive, irrevocable, world-wide license to reproduce, prepare derivative works, distribute copes to the public, and display publicly, by or on behalf of the Government, this work in whole or in part, or otherwise use the work for federal purposes.

THE TECHNICAL CONTENTS OF THIS PRODUCT WERE **NOT** PREPARED IN ACCORDANCE WITH THE EPRI QUALITY PROGRAM MANUAL THAT FULFILLS THE REQUIREMENTS OF 10 CFR 50, APPENDIX B. THIS PRODUCT IS **NOT** SUBJECT TO THE REQUIREMENTS OF 10 CFR PART 21.

ACKNOWLEDGMENTS

The Electric Power Research Institute (EPRI) prepared this report.

Principal Investigator
K. Yueh

This report describes research sponsored by EPRI and the U.S. Department of Energy, Office of Nuclear Energy Research, Development and Demonstration, Nuclear Energy Enabling Technologies (NEET) Reactor Materials Program under Award Number DE-NE0000539

ABSTRACT

Extensive evaluation was performed to determine the suitability of using SiC composite as a boiling water reactor (BWR) fuel channel material. A thin walled SiC composite box, 10 cm in dimension by approximately 1.5 mm wall thickness was fabricated using chemical vapor deposition (CVD) for testing. Mechanical test results and performance evaluations indicate the material could meet BWR channel mechanical design requirement. However, large mass loss of up to 21% was measured in in-pile corrosion test under BWR-like conditions in under 3 months of irradiation. A fresh sister sample irradiated in a follow-up cycle under PWR conditions showed no measureable weight loss and thus supports the hypothesis that the oxidizing condition of the BWR-like coolant chemistry was responsible for the high corrosion rate. A thermodynamic evaluation showed SiC is not stable and the material may oxidize to form SiO_2 and CO_2. Silica has demonstrated stability in high temperature steam environment and form a protective oxide layer under severe accident conditions. However, it does not form a protective layer in water under normal BWR operational conditions due to its high solubility. Corrosion product stabilization by modifying the SiC CVD surface is an approach evaluated in this study to mitigate the high corrosion rate. Titanium and zirconium have been selected as stabilizing elements since both $TiSiO_4$ and $ZrSiO_4$ are insoluble in water. Corrosion test results in oxygenated water autoclave indicate $TiSiO_4$ does not form a protective layer. However, zirconium doped test samples appear to form a stable continuous layer of $ZrSiO_4$ during the corrosion process. Additional process development is needed to produce a good ZrSiC coating to verify functionality of the mitigation concept.

Keywords

SiC Composite, BWR, BWR Channel

CONTENTS

LIST OF FIGURES

LIST OF TABLES

1
INTRODUCTION

The use of SiC in nuclear applications has been in development for many years. Much of the early research had been focused on high temperature gas and fusion reactor applications [1-3]. The fusion application research generated significant material characterization data that indicate the material may be stable to high neutron fluences after irradiation induced swelling saturation. The material also maintains strength to high temperatures, a property that may be useful under transients and beyond design basis accident conditions. It is only in recent years that research has begun for potential use of the material in light water reactor (LWR) reactors [4-7]. Initial effort focused entirely on fuel cladding applications but preliminary evaluations indicate significant challenges must be overcome in that application, such as developing a robust end-plug seal and a viable fuel rod design that meets all design requirements [7]. In part due to the technical challenges in designing a functional SiC based fuel rod, an examination of nuclear fuel construction was made to identify alternative potential components that could be replaced by SiC based materials. Boiling water reactor (BWR) channel was identified as a more suitable first application of SiC since its design requirements are much simpler. Expedient implementation of the material as a fuel assembly components could generate additional data to support the SiC fuel rod application.

At the time of this review, zirconium alloy based BWR fuel channels were experience severe bowing due to increased fuel utilization. The issue became more serious with longer cycles, such as the 24-month cycle typically utilized in the US BWR fleet. Excessive channel bow is primarily caused by increased hydrogen pickup on the sides of the channel that were exposed to control blades. Over the years the use of alternative zirconium based alloys have been explored with only limited success. Deformed channels can interfere with control blades insertion and thus is a safety issue, see Figure 1-1. Channel deformation can take the form of axial bow and side-wall bulge, both of which could reduce the gap between channels designed for control blade travel. SiC composites fabricated from nuclear grade fibers have demonstrate stability to high fluences without mechanical property degradation. The irradiation stability of SiC composites could offer a solution to the channel bow issue.

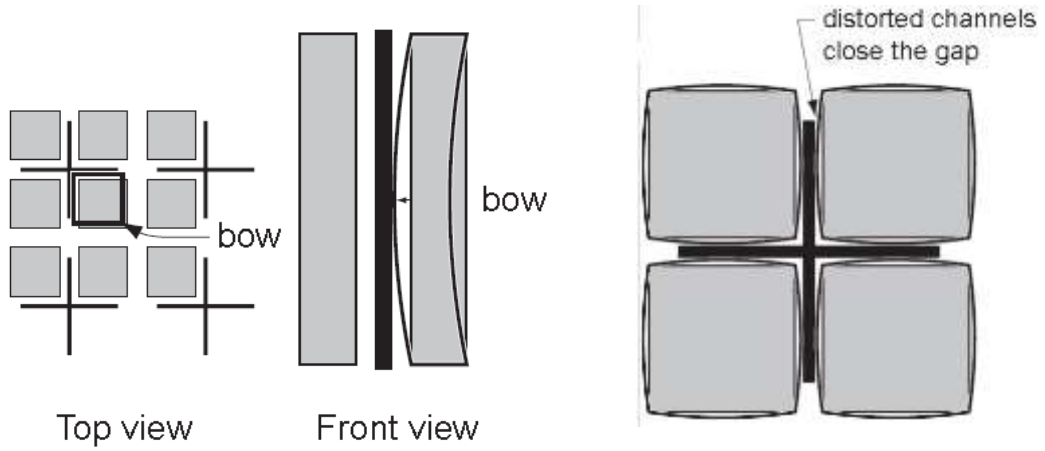

Figure 1-1 – Schematic illustrating channel bow and bulge.

After the Fukushima accident, fuel material performance under severe accident conditions gained importance and visibility. Although zirconium based channels are not heat conducting surfaces in contact with the fuel, under severe accident conditions steam cooling is very limited and the whole core heats up. Under such scenario major concerns are heat released from exothermic reaction of the zirconium based alloys with steam and hydrogen generated in the process. The energy released from the exothermic reaction increases the temperature further resulting in accelerated oxidation. Model evaluations indicate accelerated oxidation for zirconium based alloys could occur at approximately 1200°C with sufficient steam cooling. The high temperature properties of SiC delays the onset of degradation, both oxidation and mechanical strength, to temperatures closer to the melting point of UO_2 and therefore is well positioned to mitigate the two major concerns.

This report documents evaluations performed to gauge suitability of using SiC as a BWR channel material.

1.1 Feasibility Evaluation

A review of the SiC property against design requirements was conducted to identify issues that could be detrimental to the SiC BWR channel concept. The review identified three major issues that could challenge the concept: (1) corrosion rate, (2) fragmentation resistance, and (3) differential swelling induced channel bow.

1.1.1 Corrosion

The corrosion response under irradiation was thought to be a known quantity as previous irradiation testing conducted by Westinghouse and Ceramic Tubular Product (CTP) [5] showed minor weight loss after irradiation in the Massachusetts Institute of Technology (MIT) Research Reactor. Although the weight loss was low, but it is a concern from fuel performance point of view as the presence of silicate in the coolant could promote the formation of tenacious crud that could interfere with heat transfer and potentially cause fuel failures via crud induced localized

corrosion (CILC). The tests were conducted under pressurized water reactor (PWR) conditions and it was anticipated irradiation under BWR coolant conditions would yield similar weight loss. The measured weight loss was acceptable from fuel rod integrity point of view, but the release would bring the silicate levels to above the 1 parts per million (ppm) industry primary coolant guideline. The problem is silicate cannot be removed effectively via existing demineralizer or ion exchangers. Despite this issue, it is expected a solution could be found to remove excess silicate from the coolant and therefore would not be detrimental to the concept.

1.1.2 Fragmentation test

Low ductility of ceramic materials typically solicit images of fragmentation on mechanical impact. The ability to resist fragmentation and dispersal of fragments is a key requirement to maintain functionality and avoid introducing a foreign material issue that could lead to fuel failure. To meet the requirement the BWR channel must be able to survive normal handling impacts without damage and only experience limited fragment dispersal in fuel handling accident impacts. A test article with a cross-section slightly smaller than a commercial BWR channel was fabricated by the chemical vapor deposition (CVD) process using Hi-NicalonTM Type S fiber [7]. The fibers are braided at an angle to improve fracture resistance. All of the materials used in tests described in this report were sections from this channel box.

1.1.2.1 Test article fabrication

The composite SiC_m-SiC_f channel box was produced with near stoichiometric Hi-Nicalon Type S SiC fiber in a SiC matrix produced by chemical vapor infiltration (CVI). A thin pyrolytic carbon (0.10+/-0.05 microns) was applied to the fiber prior to matrix densification. This composite construction has been previously shown to be radiation stable. The fiber preform was constructed of four layers of Hi-Nicalon Type S totaling 0.06-inch thickness. The innermost and outermost layers were constructed of triaxial braids formed continuously around a mandrel with the geometry of the channel box inner mold line. The two layers between the braided layers were formed from high areal weight Hi-Nicalon Type S fabric (8 harness satin construction at 360 g/m2) with an overlap joint such that the expected axial strength was >30 ksi. After preforming, a pyrolytic carbon fiber coating was applied by the thermal decomposition of hydrocarbons at elevated temperature and reduced pressure. SiC matrix densification was performed by CVI using the thermal reduction of methyltrichlorosilane to beta phase silicon carbide. CVI processing with uniform deposition on all preform surfaces was continued until ~10% residual porosity remained. A photograph of a section of the channel is show in Figure 1-2.

Figure 1-2 A section of test sample.

The test article had a 10 cm squared cross-section and with a wall thickness of approximately 1.5 mm. A 50 cm long section was used in an impact test.

1.1.2.2 Test conditions

Three types of impact loading conditions, based on actual fuel handling equipment operational practices, were considered.

Normal Loading Impact: The component must survive normal handling impact loads without damage. This scenario is applicable to normal fuel movement where the SiC channel may come into contact with other fuel assemblies, core baffle or fuel storage structures. An impact velocity of 1.8 meter/minute is defined for this condition. A single impact location at middle location of the fuel assembly is assumed. The SiC based channel must not sustain any damage as the continued use of the component is expected.

Full Speed Horizontal Impact: The second scenario involves a fuel movement accident in which fuel moving horizontally at 18.3 meter/minute impacts a stationary object. A single impact location at the middle of the fuel assembly is assumed. The fuel would most likely not be used after such an accident and so limited damage may be allowed.

Drop Impact: The third scenario is the most severe and it simulates the side-impact of an assembly tipping over on its side in water and impacts 10 channel handles. The top span with the largest drop distance of 3.66 meter was used to calculate the kinetic energy at the point of impact. This energy was then used to calculate an equivalent impact velocity of a full mass assembly in air. Damage under this scenario is expected but fragmentation would not be acceptable.

The energy of impact was scaled back 40% for all three scenarios because the nominal dimension of the test article is smaller than actual channel. Only one test article was available and it was impacted three times in the order listed above.

1.1.2.3 Test apparatus

Impact tests were conducted in air with the SiC test article attached to the middle of a simulated BWR fuel assembly, see Figure 1-3. The facsimile fuel assembly has the same mass and external dimension of a typical BWR fuel assembly. During a test, the simulated assembly is suspended on a bridge crane and energy is imparted to the system by pulling back the bottom of the assembly and then releasing it to impact one of two types of fixed impacting surfaces. A plate approximately 15 cm in height was used for conditions 1 and 2 and a production BWR channel handle was used for condition 3.

(a) (b) (c)

Figure 1-3 (a) Model of test apparatus, (b) flat impact surface used for test conditions 1 and 2, and (c) BWR channel handle used as an impact for condition 3.

1.1.2.4 Test results

No visible damage was detected after the first impact (condition 1). A small amount of material was dislodged from the surface on the second impact (condition 2), but no visible structural damage. The test article was punctured on the 3rd impact (condition 3). Debris generated from impacts 2 and 3 as well as an image of the puncture from impact 3 are shown in Figure 1-4.

The test article performed quite well from fuel fragmentation resistance point of view. Most of the debris generated from the 3rd impact came from the channel handle cutting into the side-wall of the test article. There was no crack propagation even with the puncture. Preliminary consensus is that the debris generated would be acceptable.

(a) (b) (c)

Figure 1-4 (a) Debris generated from the 2nd impact, (b) puncture after 3rd impact, and (c) debris generated from the 3rd impact.

1.1.3 Irradiation induced swelling

Silicon carbide is known to swell under neutron irradiation but saturates quickly after only 1 displacement per atom (dpa). Since some fresh channels will experience significant flux gradient, differential volumetric swelling may introduce a temporary channel bow. The magnitude of channel bow from the differential volumetric swelling must be smaller than the design limit. An evaluation was performed using an actual BWR core design and literature irradiation property data. The evaluation indicates a flux differential of approximately 25% is acceptable. For the specific core used in the evaluation approximately a dozen fresh channels experience flux gradient between 25-29%. In reality the flux gradient at the beginning of a cycle is typically less than calculated since the power gradient within an assembly won't fully develop until later in the cycle. The condition was deemed acceptable as minor core design changes, detailed evaluation or the use of a few metal channels could mitigate potential bow from a higher flux gradient.

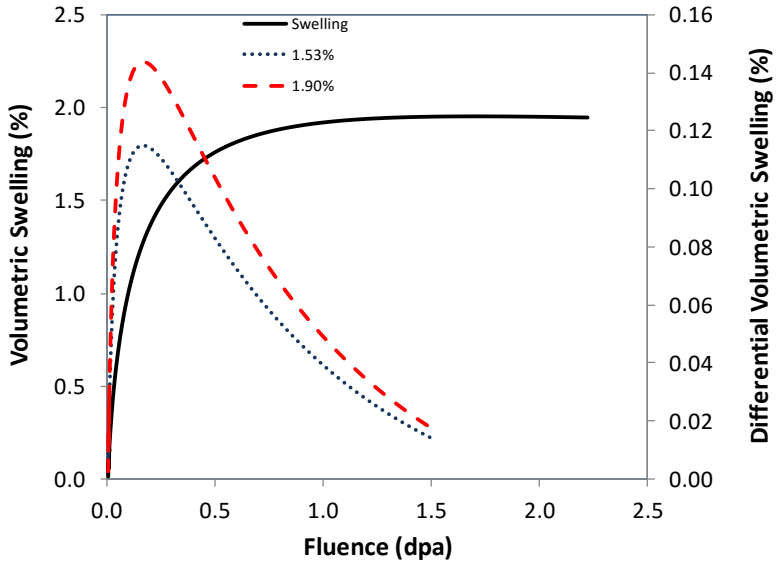

Figure 1-5 – Volumetric swelling and calculated volumetric swelling differential.

1.2 Economic Study

The impact of lower neutron capture cross-section of SiC was evaluated from reactivity and economic perspectives for channel wall thicknesses of 2, 2.5 and 3 mm at a nominal core void fraction of 40%. The lattice physics transport code CASMO4E was used to estimate k_{inf} as a function of burnup for a BWR fuel assembly. It consists of a 10x10 square array of fuel rods, with 8 of the central rods replaced by 2 large water rods. A complete assembly would have some part length fuel rods and several different axial zones of varying fuel enrichment and gadolinia loading. For this scoping analysis, only a typical axial zone toward the center of the assembly is modeled. Lower fuel rod enrichments are used for peripheral than for interior rods to minimize power peaking. The typical Zircaloy channel thickness in GE6 reactors is 100 mils (2.5 mm), although 80 mil (2 mm) channels have also seen some use. The base channel thickness used here is 100 mils. As the appropriate thickness for SiC channels is unknown, the same base dimension is used, but variations of ± 25% were also considered. This work does not include any evaluation of the thermal-hydraulic or mechanical implications of using a SiC channel.

As expected all three cases showed positive reactivity change that increases with burn-up relative to a 2.5 mm zirconium based channel. An evaluation of the reactivity increase indicates the fuel enrichment may be decreased by approximately 0.1% for equivalent core reactivity, translating to approximately $3 million in savings per batch of fuel assemblies. A sensitivity evaluation of the effect of SiC channel on the void coefficient of reactivity was also investigated. Relative to a 2.5 mm zirconium channel, the results indicates positive change in the coefficient for 2 and 2.5 mm channel thickness and slightly negative for the 3 mm thick channel.

Figure 1-6 displays k_{inf} vs. burnup at 40% void for the nominal case with a zirconium alloy channel box thickness of 2.5 mm and SiC cases with channel box thicknesses of 2.0 mm, 2.5 mm, and 3.0 mm.

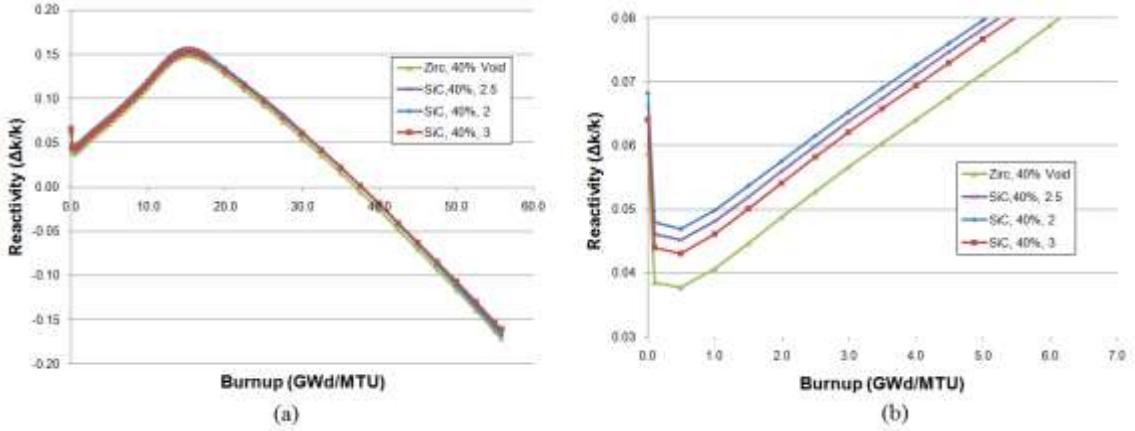

Figure 1-6 (a) k_{inf} vs. burnup for a GE-11 BWR assembly with 2.5 mm Zircaloy and 2.0 mm, 2.5 mm, and 3.0 mm SiC channel boxes, all at 40% void. (b) Close-up of (a) from 0.0 to 7.0 GWd/MTU

As seen in Figure 1-6(a), k_{inf} follows the usual trend for all cases, experiencing a sharp decrease at beginning of life (BOL) due primarily to xenon poison ingrowth, followed by increasing reactivity due to burnable poison depletion until ~15 GWd/MTU, and decreasing nearly linearly thereafter. Figure 1-6(b) shows a closeup of the low burnup region, where it is apparent that early

in life all three SiC cases increase the reactivity, by amounts ranging from about half a percent to nearly a percent. The thinner SiC channels yield greater reactivity gain at BOL
As the assembly burns, all three SiC channels retain their reactivity advantage over Zircaloy, but their rankings change. Figure 1-7 shows the reactivity gain of each SiC case relative to the Zircaloy as a function of burnup.

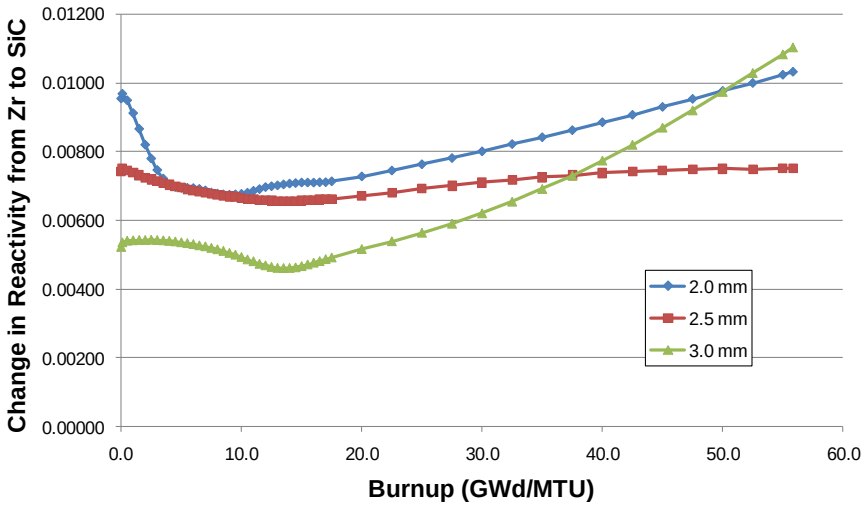

Figure 1-7 Difference in reactivity between 2.5 mm-thick Zircaloy channel and SiC channel sof 2.0, 2.5, and 3.0 mm thickness for a GE-11 assembly at 40%void

As shown in Figure 1-7, the SiC channel box with a thickness of 2.5 mm (same as the zirconium alloy) has a reactivity 0.0074 Δk/k greater than the nominal zirconium alloy channel box at BOL. This is because SiC has a lower microscopic neutron absorption cross section than zirconium for the energy range 0.1 eV to 3 MeV, as well as a lower macroscopic absorption cross section, since its density is less than half that of zirconium alloy [9]. It also provides a little more neutron moderation.

The SiC channel box with a thickness of 2 mm has a reactivity 0.0095 Δk/k greater than zirconium alloy at BOL, which is 0.00213 Δk/k greater than for the SiC channel box with 2.5 mm (nominal thickness). The additional increase in reactivity for the 2 mm vs. the 2.5 mm channel box is due to two complementary factors: (1) decreased absorption in the 2 mm box because of the 20% decrease in thickness; and (2) increased moderation due to the increased thickness of the water gap.

The SiC channel box with a thickness of 3 mm has a reactivity 0.0052 Δk/k greater than zirconium alloy at BOL, but 0.0022 Δk/k less than the SiC channel box with a thickness of 2.5 mm. Again, this is because the 3 mm SiC channel box experiences more neutron absorption and less moderation than the 2.5 mm SiC box. However, since the 3 mm channel box's reactivity is still greater than the zirconium alloy's reactivity, this indicates that the reactivity gain due to the reduced microscopic cross section of SiC is a more dominant effect than the reduction in moderation due to a thinner water gap.

At end of life (EOL), a different trend is encountered. The 3 mm SiC channel box has the greatest reactivity gain, 0.011 $\Delta k/k$ relative to the Zircaloy. The 2 mm SiC channel box has a reactivity 0.010 $\Delta k/k$ greater than Zircaloy, and the 2.5 mm SiC channel box has a reactivity 0.0075 $\Delta k/k$ greater than Zircaloy. The 3 mm channel box has the greatest reactivity at EOL probably because of its slightly harder spectrum due to lessened moderation leads to additional plutonium ingrowth with burnup.

Similar spectrum effects as a function of burnup are seen in the standard depletion calculations performed during core design; when such depletion calculations are performed at 0, 40, and 70% void, the 70% void curve (i.e., minimum moderation) crosses the other two curves at high burnup.

2 TEST PROGRAM

The test program with partial US Depart of Energy (DOE) funding under the Nuclear Emergent Energy Technology (NEET) program is primarily focused on generating irradiation data using prototypical channel material architecture at prototypical operating temperatures. Since the initiation of the project additional out-reactor tests were added. The goal of the test program was to generate sufficient test data to support a SiC_m-SiC_f composite BWR channel demonstration in a commercial nuclear reactor. The test scope included the following goals

a) Characterize irradiation induced swelling at prototypical BWR coolant conditions
b) Determine the thermal/irradiation creep rate
c) Characterize corrosion behavior in a BWR-like water chemistry
d) Small scale demonstration in the Oak Ridge National Laboratory High Flux Isotope Reactor (HFIR)
e) Generate non-irradiated characterization data
    i. Tensile strength
    ii. Flexure strength
    iii. Density
    iv. Fatigue
    v. High temperature oxidation
    vi. Thermal quench
    vii. Thermal conductivity
    viii. Surface roughness effect on pressure drop

Objectives d, e(vii) and e(viii) were not pursued due to unfavorable corrosion test results from the MIT research reactor.

2.1 Test samples preparation

Test samples were sectioned from the channel box fabricated per section 1.1.2.1 to dimensions tabulated in Table 2-1. A photograph of a typical sample is shown in Figure 2-1.

Figure 2-1 – Test coupon

Table 2-1 Test temperature and sample dimension

Test	Temperature (°C)	Orientation	Length (mm)	Width (mm)
Swelling	260/280	Transverse/axial	24	4.5
Corrosion	280	Transverse/axial	76	10
Creep	280	Transverse/axial	89	10
Tensile	RT	Axial	101.6	8.89
	300°C	Axial	127	15.24
Flexural	RT	Transverse/axial	76.2	6.35
	300	Transverse/axial	50.8	6.35
Fatigue	300	Axial	152.4	13.97
LOCA quench	1100	Whole X-section	75	
Steam oxidation	>1500	N/A	50.8	12.7

2.2 Non-irradiated Testing

2.2.1 Tensile and flexural

Flex tests were conducted per ASTM standard C1341. Room temperature flexural specimens were tested in four point bending – 1/4 point with a span of 63.5 mm, while the high temperature flexural tests were four point - 1/3 point with a span of 24.9 mm. Testing was performed on specimens machined in both the axial and transverse directions, for both temperatures. Load and displacement data were recorded for all tests. Both stress and strain were calculated using the span length and the average gage section thickness and width. Tension testing was performed at both room temperature per ASTM C1275 and at 300°C per ASTM C1359. Load and strain data were recorded for all tests and stress was calculated from average gage section thickness and width measured before the test.

The test results expressed as average of individual tests are tabulated in Table 2-2. The measured strengths are significantly lower than that of zirconium based metal alloys currently in use. It is also lower relative to values reported in literature for SiC composites. The low strength could be attributed to the lower fiber content and this implies it could be improved in the final product when a higher fiber fraction could be achieved with a thicker wall. Furthermore, the design requirement of a channel is rather simple and the limiting loading condition is during a seismic event. As the loading cycles is limited in a seismic event, fatigue test results shown in the next section indicate loading beyond the proportional limit (PL) in these special situations would be permissible.

Table 2-2 Flex and tensile test results.

Test Type	Temperature	Orientation	σ (MPa)	σPL (MPa)	εf (%)	εPL (%)
Flex	RT	Axial	283	106	0.56	0.08
		Transverse	276	108	0.39	0.06
	300°C	Axial	424	177	0.69	0.16
		Transverse	327	152	0.74	0.16
Tensile	RT	Axial	168	73	0.36	0.03
	300°C		150	72	0.36	0.03

2.2.2 Fatigue

Fatigue testing was performed using 152 mm "dogbone" coupons. It was determined from room temperature tensile testing that the proportional limit strength of the material was 72 MPa. Fatigue testing was started at a stress level ~10% of the proportional limit strength (6.9 MPa) and increased by 10% every 1000 cycles until a maximum run-out of 25,000 cycles was achieved. Testing was performed at 10 Hz. Test results, tabulated in Table 2-3, indicate all of the test samples survived a large number of cycles above the proportional limit stress. This further reinforces the use of the strength beyond the proportional limit.

Table 2-3 Fatigue test results.

Specimen #	Temperature	Total Cycles	Final Stress (MPA)	Type of Failure
1	300°C	19,963	138	Angled in gauge area
2		25,000	173	--
3		25,000	173	--
4		25,000	173	--

2.2.3 Density

Bulk density and Archimedes densities were measured on room temperature and elevated temperature tensile specimens as well as the fatigue specimens. These were chosen as their measured densities are most representative of the panel as a whole due to the fact that they have the largest volume. The results are shown in Table 2-4.

Table 2-4 Measure density.

Sample Type	Bulk Density (g/cm^3)	Archimedes' Density (g/cm^3)
RT Tensile	2.64	2.93
ET Tensile	2.77	2.93
Fatigue	2.76	2.91
Average	2.73	2.92

2.2.4 High temperature steam oxidation

The high-temperature steam oxidation tests were performed in the high-temperature furnace module of the severe accident test station at ORNL. The details of the experimental apparatus are provided elsewhere [3]. Briefly, the experimental setup consists of steam flowing inside an alumina tube heated within two $MoSi_2$ furnaces. As shown in Figure 2-2, the specimen is hung using an alumina rod from the top of the test tube. The steam produced inside the boiler, initially enters the preheat furnace and subsequently flows past the specimen centered in the high-temperature furnace enabling exposure at the target test temperature.

During the temperature ramp the specimens were exposed to flowing argon and did not experience any oxidation. Once the target temperature was reached the environment was switched from that of inert gas to pure steam. The steam flow velocity was controlled with the rate of water injection into the boiler using a pneumatic pump. Figure 2-3 shows a typical temperature profile during a 4-hour steam exposure test.

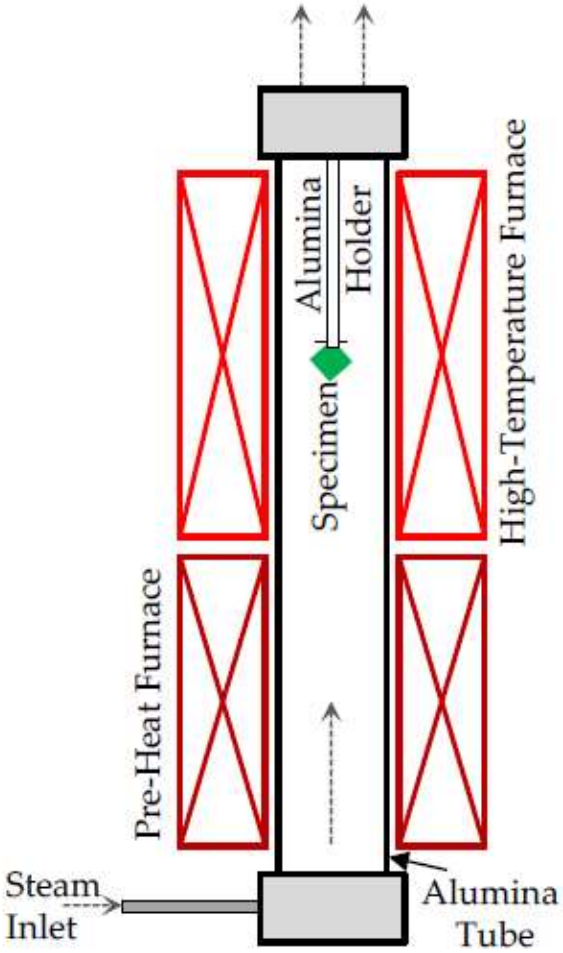

Figure 2-2 Experimental setup during high-temperature steam oxidation test [3]

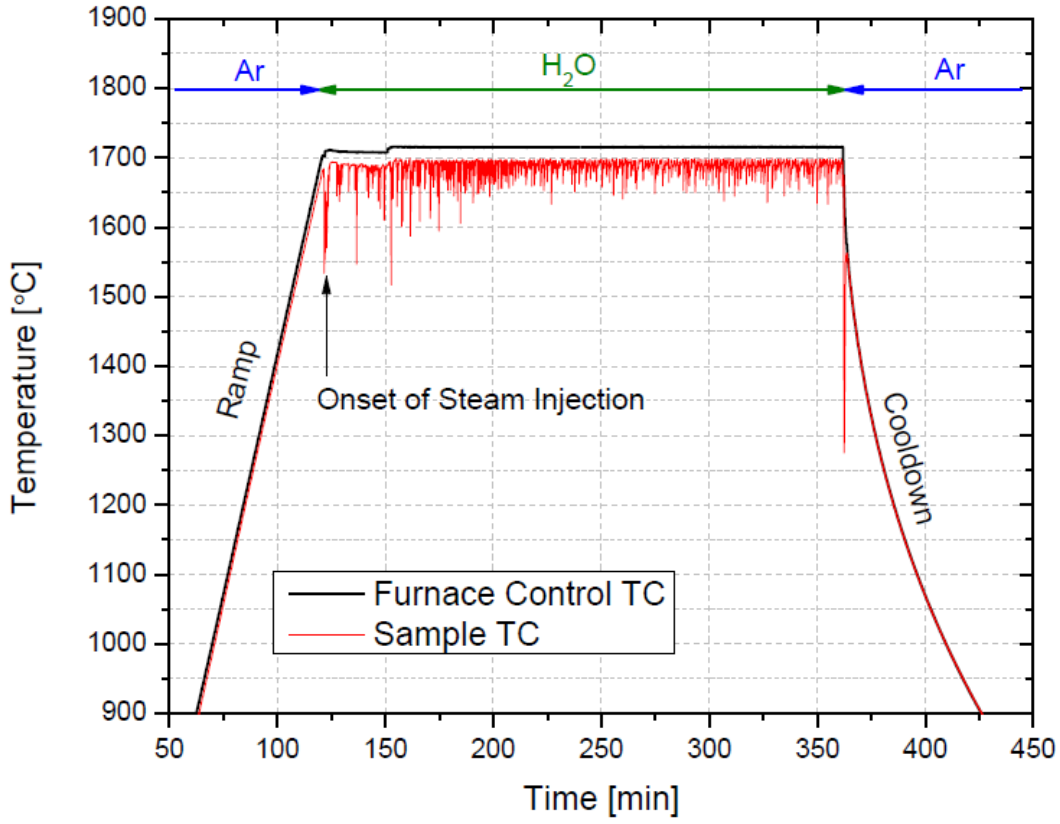

Figure 2-3 Experimental furnace and specimen temperature profile during the 1700°C steam oxidation.

The results from the high-temperature steam oxidation tests are summarized in Table 2-5. While a slight mass gain as a result of oxidation was observed at 1600 °C, a slight mass loss was recorded for the specimen exposed to 1700 °C steam. No significant mass change beyond the uncertainty level in the measurement was detected after the 4-h 1200 °C exposure. The results are also summarized in Figure 2-4.

Table 2-5 Summary of mass and dimensions for the SiC/SiC composite specimens exposed in the high temperature steam oxidation experiments for 4 hours.

ID	Temperature [°C]	Gas Velocity [cm/s]	Dimensions [mm]			Area [cm^2]	Initial Mass [g]	Final Mass [g]	Unit Mass Change [mg/cm^2]
			Length	Width	Thickness				
1	1200	50	50.93	12.81	1.76	15.29	2.61911	2.62133	0.15
2	1200		50.94	12.81	1.91	15.49	2.75012	2.74801	-0.14
3	1600	64	51.17	12.82	1.88	15.53	2.55288	2.55713	0.27
4	1600		51.17	12.80	1.90	15.53	2.69258	2.69616	0.23
5	1600		50.73	12.79	1.81	15.28	2.66482	2.67101	0.41
6	1700	68	50.90	12.80	2.02	15.60	2.71080	2.69615	-0.94

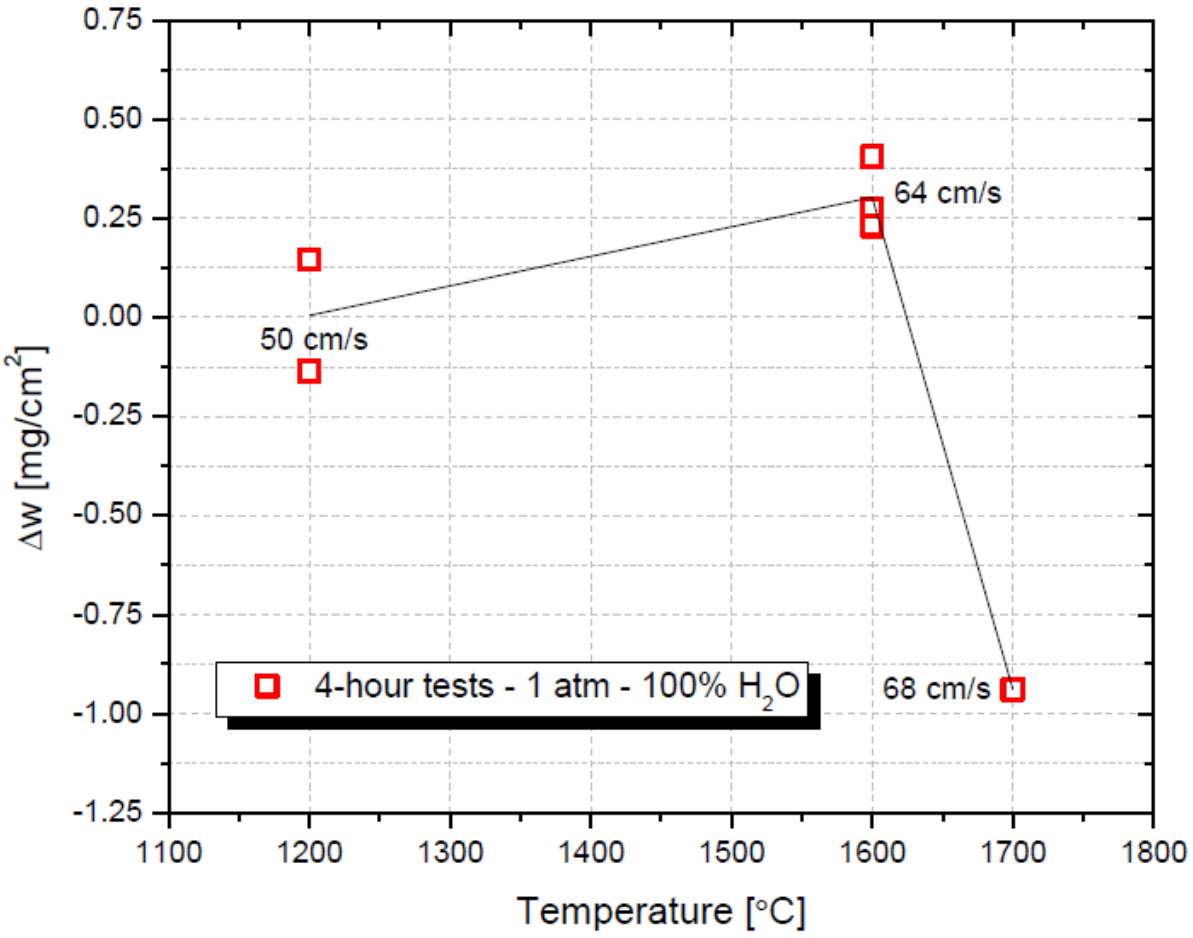

Figure 2-4 Magnitude of mass change per unit area as a function of temperature for 4 hour steam exposure of SiC/SiC composite specimens.

Visual appearance of test samples before and after the high temperature steam exposure are shown in Figure 2-5. The photographs do not indicate a change in the fiber dimensions, consistent with the weight measurements.

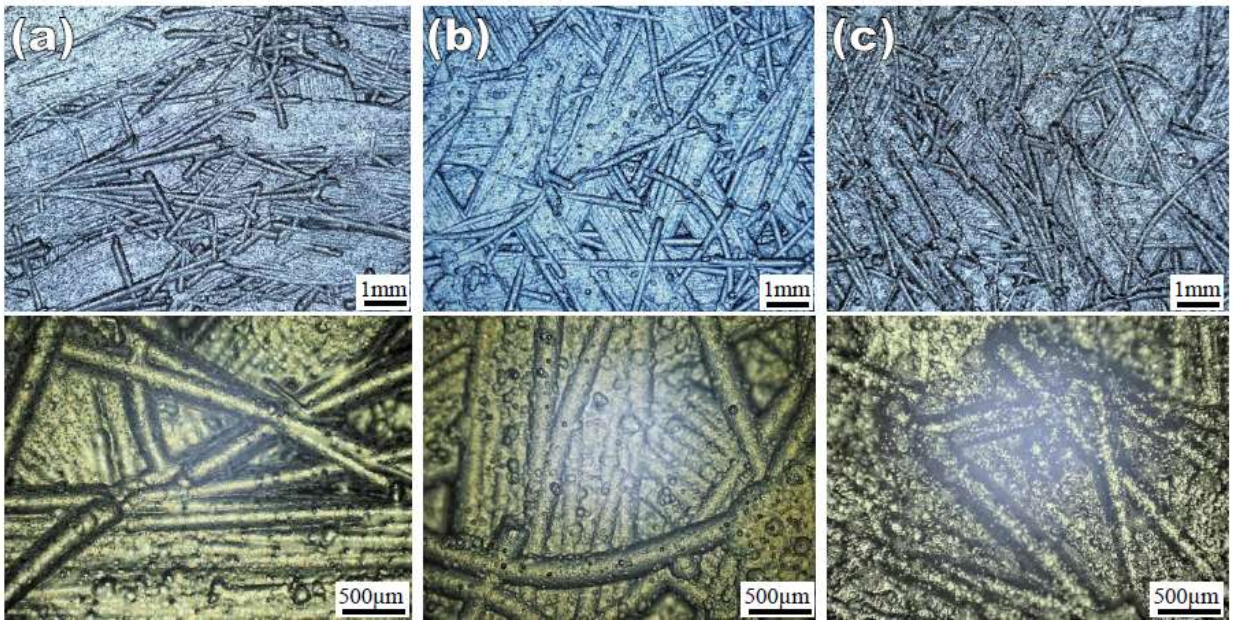

Figure 2-5 Optical micrographs of SiC/SiC composite materials before testing (a), and after 4-h steam exposures at 1600 °C (b), and 1700 °C (c).

2.2.5 Thermal quench

SiC/SiC composite channel box quench testing was performed using a simple procedure consisting of a rapid temperature ramp, a 400 s hold at max temperature, rapid cooling to ~850°C, and subsequent drop into a water reservoir. Since the channel box was a transverse cross section of what is envisioned in the BWR fuel assembly application, its cross-sectional dimensions were typical of such structures: ~4”×4”. Accordingly, a specialized furnace was used to accommodate the geometry of the specimen and deliver desirable target temperatures. The furnace was an infra-red (IR) heating module with a 6” diameter quartz tube extending into the heat zone. Prior to specimen insertion, the furnace temperature was set to 1100°C. The channel box specimen was placed on top of a glass slide with an S-type thermocouple held between the two and in contact with the channel box wall. The glass slide was moved into the heat zone and in this manner a very rapid temperature ramp rate, consistent with what is expected under a large-break loss of coolant accident (LBLOCA) scenario was achieved. Once the specimen was at the center of the heat zone, it was held there for ~400 s. After this holding period was complete, the specimen was extracted outward and then quickly dropped into a water reservoir. The channel box entered the water vertically, consistent with what is expected to occur under core quench (water rising vertically against the channel box wall). The temperature profile during the ramps is shown in Figure 2-6. The test in its entirety was performed in an air atmosphere.

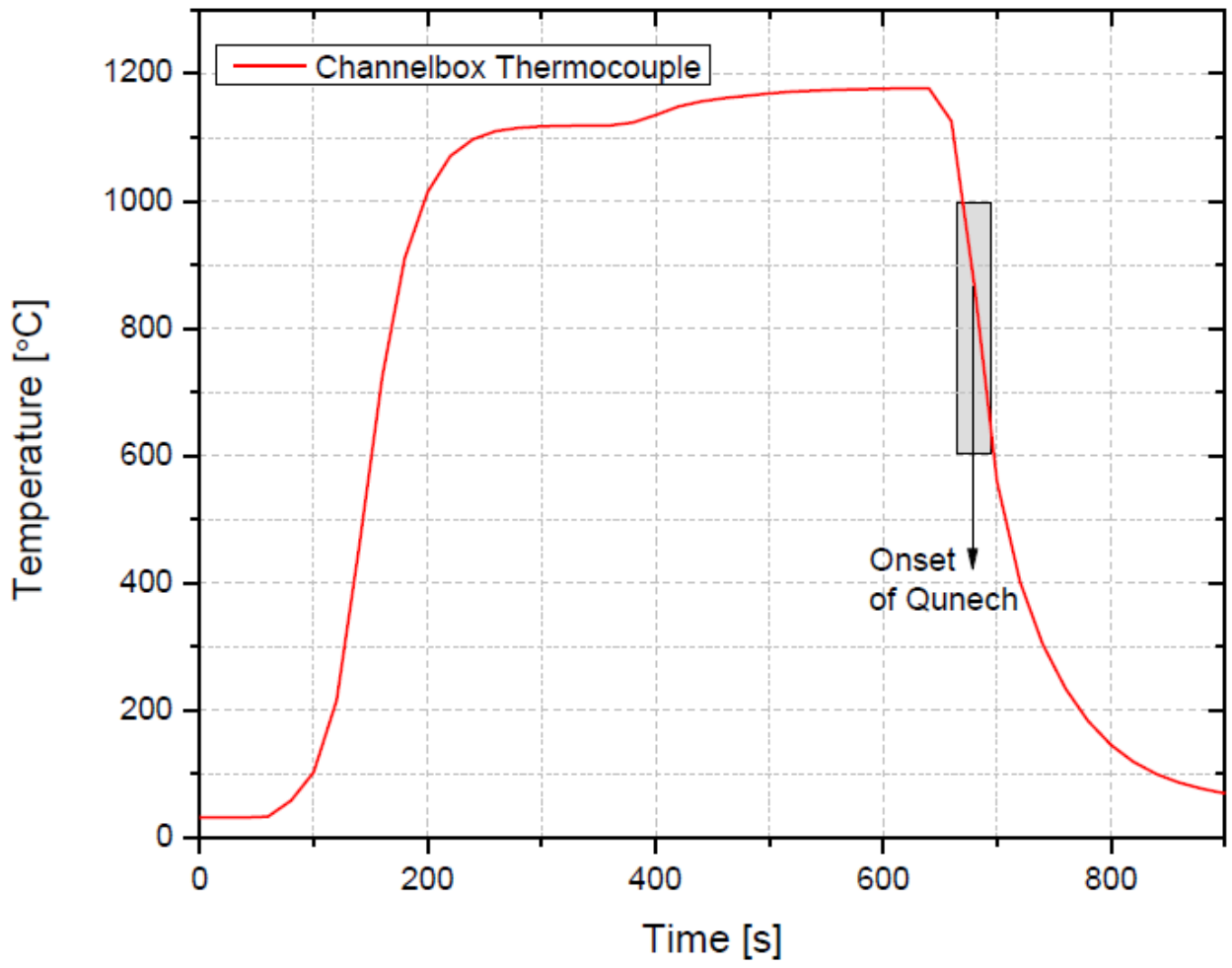

Figure 2-6 Channelbox temperature profile prior to the quench test.

The channel box specimen with dimensions summarized in Table 2-6 was subject to the temperature ramp and the subsequent room-temperature water quench test as described in Figure 2-7. A very limited mass loss was measured for the specimen after the quench test. No sign of debris or chips was found inside the water reservoir following the quench. Figure 2-7 shows the channel box specimen during the high-temperature air exposure and subsequent to the quench.

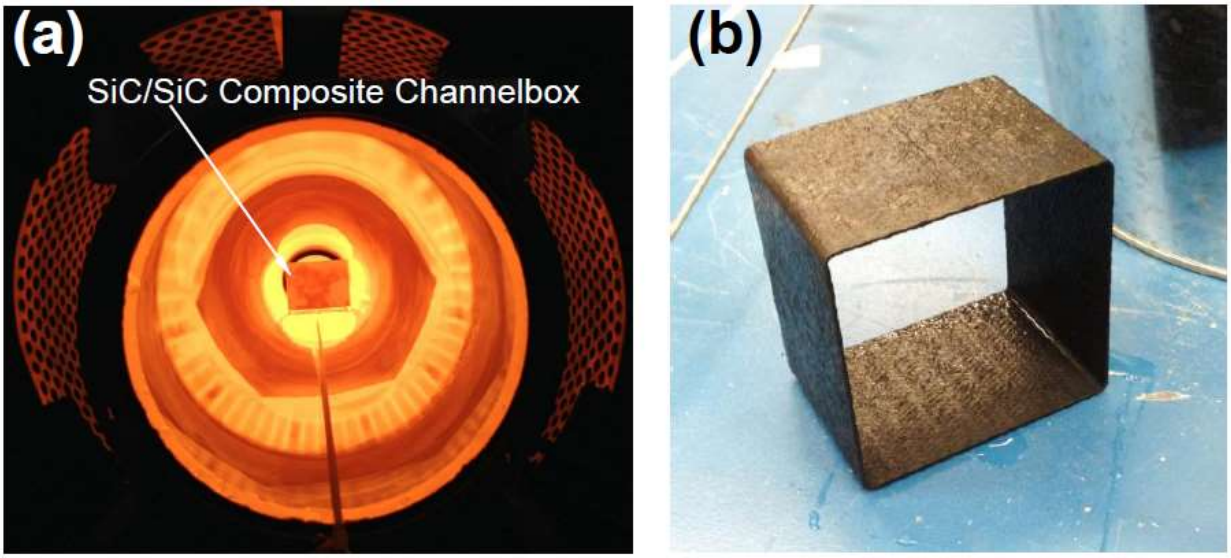

Figure 2-7 a) SiC/SiC composite channelbox inside the quartz tube of the IR furnace at ~1150°C. b) Channelbox after quench in RT water.

Table 2-6 Summary of mass and dimensions for the SiC/SiC composite channelbox quench experiment.

Dimensions [mm]*			Mass [g]		Total Mass Change [mg]
Length	102.92	± 0.47	Prior to quench test	139.9235	-38.5
Width	102.71	± 0.03			Unit Mass Change [mg/cm^2]
Height	76.25		Post-quench condition	139.8850	
Thickness	2.11	± 0.10			-0.06

*No change in dimensions in the post-quench condition.

2.3 Irradiation Testing

Irradiations were conducted in the High Flux Isotope Reactor (HFIR) and the Massachusetts Institute of Technology research reactor (MITR). The HFIR irradiation is primarily targeted to generate irradiation induced swelling data at various fluence levels since its rabbit facility allows for convenient sample insertion and withdrawal. The MITR irradiation is primarily targeted to characterize the material corrosion and creep behavior with a secondary goal of irradiation induced welling. Since the HFIR neutron flux is much higher compared to a commercial reactors the validity of the test data to commercial LWR condition need be verified. This verification could be satisfied by measuring the dimensional changes of the MITR test coupons.

HFIR irradiation was conducted using the hydraulic rabbit irradiation facility. The irradiation vehicle was designed to target samples temperatures of 260 and 280°C. The fast neutron flux at the specimen locations were ~1 x 10^{19} n/m^2/s. The equivalence of 1 dpa in SiC with a fast fluence 1 x 10^{19} n/m^2 (E > 0.1 MeV) is assumed hereafter. The irradiation vehicles were

designed for temperatures of 260°C or 280°C. The conditions of irradiation are summarized in Figure 2-7.

2.3.1 Irradiation Induced Swelling

The specimens were machined from a prototypical channel box made of Hi-Nicalon™ Type S near-stoichiometric SiC fiber-reinforced, chemically vapor-infiltrated (CVI) SiC matrix composite with pyrolytic carbon (PyC) fiber/matrix interphase. Rectangular coupon specimens measuring nominally 24 mm (length) x 4.5 mm (width) x 1.3 mm (thickness) were machined from the flat wall sections of the channel box in the axial (specimen length in parallel with the box axial length) and the transverse (specimen length in parallel with the box width) orientations. These specimens are referred to as axial and transverse specimens hereafter. Photographs of an axial and a transverse specimens are shown in Figure 2-8.

Figure 2-8 Axial (left) and transverse (right) coupon specimens used in this research.

Irradiation of these test coupons were performed in the High Flux Isotope Reactor (HFIR) using its hydraulic rabbit irradiation facility. The facility is designed to enable rapid insertion and removal of small irradiation vehicles in and out of the flux trap of HFIR at any time during the reactor operation to achieve the exact desired neutron dose. Seven hydraulic rabbit capsules were designed, built, and irradiated for the present research as summarized in Table 2-7. Each capsule contained four axial specimens, four transverse specimens, and two additional specimens of high purity chemically vapor-deposited (CVD) SiC beams as reference specimens.

Table 2-7 Rabbit capsules irradiated in present research.

ID	Target Temperature (°C)	Target Dose (dpa)	HFIR Position	Fast Flux (n/cm^2-s, E > 0.1 MeV)	Irradiation Duration	Fast Fluence (n/cm^2, E > 0.1 MeV)	Total DPA
EPRI01	280	0.01	HT-5	8.90E+14	3.12 hr	1.00E+19	0.0100
EPRI02	280	0.03	HT-5	8.90E+14	9.36 hr	3.00E+19	0.0300
EPRI03	280	0.1	HT-5	8.90E+14	31.21 hr	1.00E+20	0.1000
EPRI04	280	0.3	HT-5	8.90E+14	3.90 days	2.99E+20	0.2999
EPRI05	280	1	HT-5	8.90E+14	13.00 days	1.00E+21	0.9996
EPRI06	260	0.03	HT-5	8.90E+14	9.36 hr	3.00E+19	0.0300
EPRI07	260	0.1	HT-5	8.90E+14	31.21 hr	1.00E+20	0.1000

Dimensions of the specimens were measured by two independent methods: using a precision micrometer unit and by a digital microscopy. The micrometer used was equipped with a high precision linear variable differential transformer (LVDT) and was maintained calibrated to an accuracy of ±0.1 micron at all time through a calibration procedure using standard gauge blocks incorporated in the specimen measurement protocol. All three dimensions of the rectangular coupon specimens were measured with the micrometer. The digital microscopy was used to verify consistency between the micrometer measurement and the digital microscopy measurement of distances between pairs of laser-engraved markings on both faces of the test coupons. The precision and the repeatability of this measurement are ±1 micron and ±3 microns, respectively.

Results from the micrometer measurements for the changes in length by micrometer, axial dimensions by measurement microscopy, width by micrometer, and thickness by micrometer are presented in Figure 2-9, Figure 2-10, Figure 2-11, and Figure 2-12, respectively. There was no significant or systematic difference in linear swelling noticed between the axial and transverse specimens of the composite material. Moreover, no significant or systematic difference was detected between the composite samples and the monolithic CVD SiC samples. As shown in Figure 2-9 and Figure 2-10, the axial swelling exhibited the well-known dose-dependent build-up behavior. Data scatter within the identical irradiation condition is likely caused by either or both of the slight specimen-to-specimen variations in the actual irradiation temperature and possible measurement error.

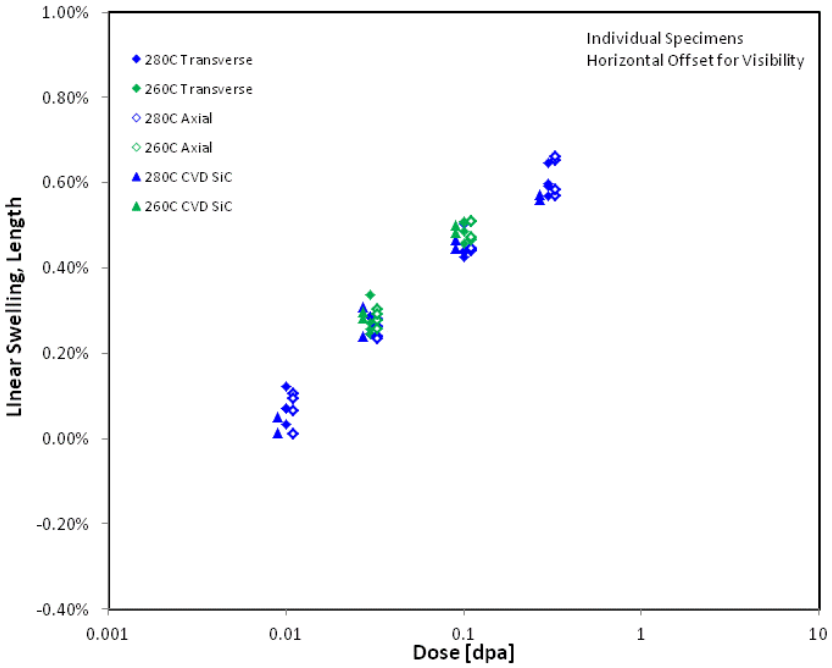

Figure 2-9 Change in specimen length as a function of dose. Data points correspond with length changes measured for individual specimens. Actual doses within each of four dose groups are identical (horizontally offset for visibility).

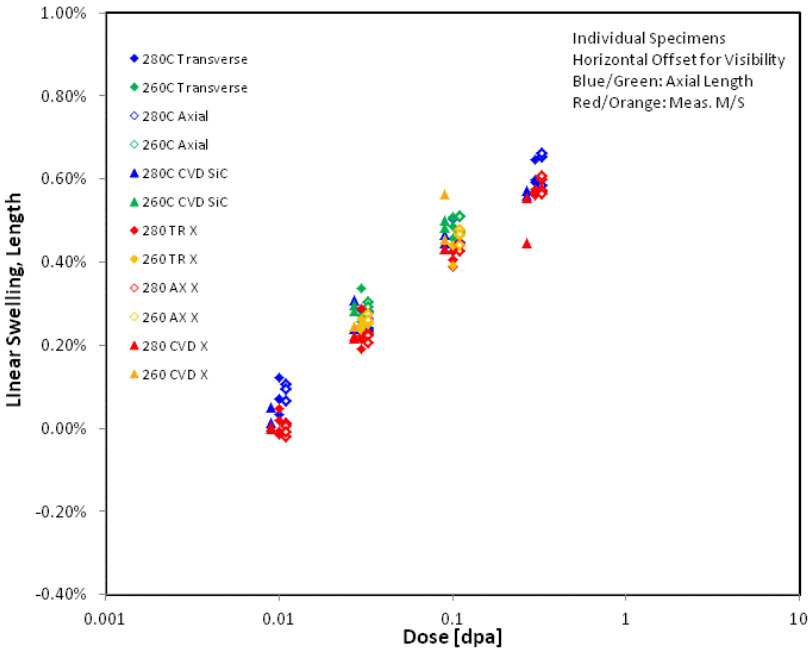

Figure 2-10 Comparison of length changes between micrometer measurement of total specimen length (blue and green symbols) and digital microscopy measurement (red and orange symbols.) Actual doses within each of four dose groups are identical (horizontally offset for visibility).

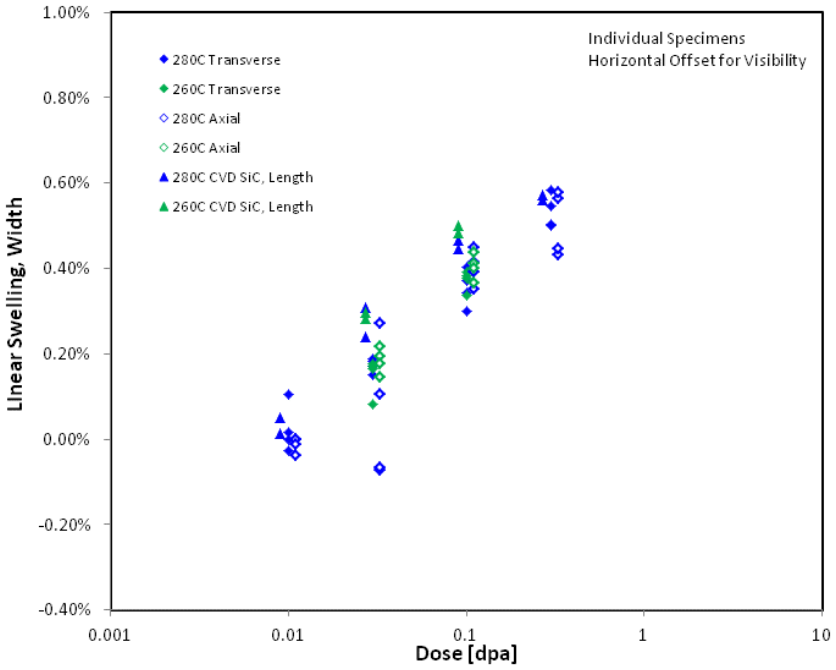

Figure 2-11 Change in specimen width as a function of dose. Data points correspond with length changes measured for individual specimens. Actual doses within each of four dose groups are identical (horizontally offset for visibility).

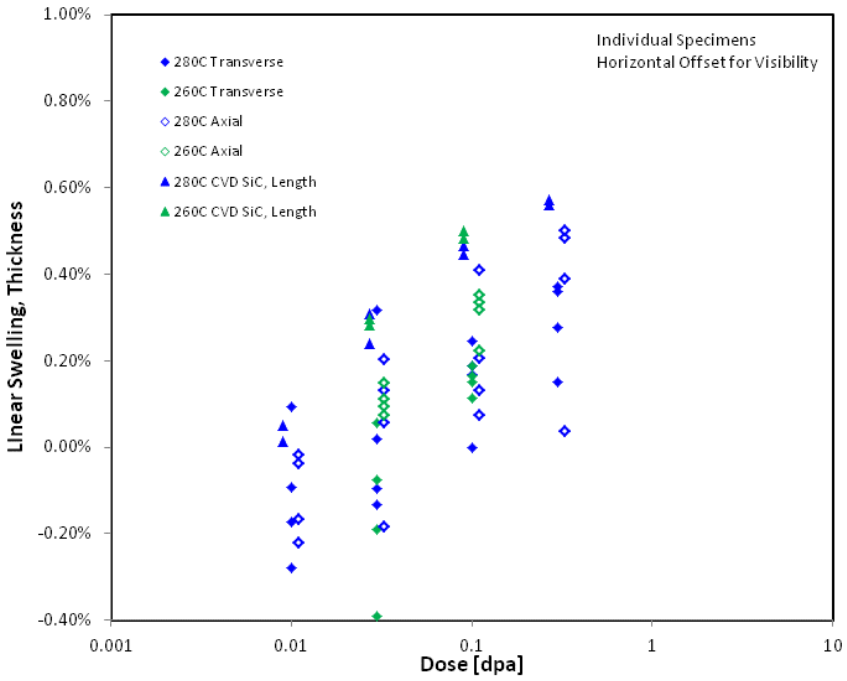

Figure 2-12 Change in specimen thickness as a function of dose. Data points correspond with length changes measured for individual specimens. Actual doses within each of four dose groups are identical (horizontally offset for visibility).

It is interesting to note the systematic difference in linear swelling in the specimen width between the composite and the CVD samples, with the composite samples showing slightly reduced swelling. Moreover, the specimen thickness is indicating even greater discrepancy between the composite and the CVD samples. It is noteworthy that 1) the specimen-to-specimen scatter in composite width after irradiation appears significantly greater than before irradiation and that 2) the composite thickness are exhibiting contraction (negative swelling on plot) at low doses. These observations imply that the Hi-Nicalon Type S fibers undergo irradiation-induced swelling in a different manner from that of high purity and fully crystalized beta-phase SiC; however the in-plane dimensions of two-dimensionally fiber-reinforced CVI SiC-matrix composites do not seem to be influenced by the slightly reduced swelling magnitude for the reinforcing fibers when the absolute dimension is greater than several repeating units for the fiber architecture.

Dimensional evolutions for Hi-Nicalon Type S SiC fiber-reinforced, CVI SiC matrix composite and high purity CVD SiC were determined in a temperature range 260 – 280 °C as a function of fast neutron dose, through the irradiation of a series of hydraulic rabbit capsules in HFIR. The result indicated equivalence in linear swelling magnitude between the composite and CVD SiC along the longitudinal orientation of coupon specimens. Slight yet systematic differences between the two materials' dimensional evolutions were noted along the specimen width and thickness.

Due to the vastly different fast neutron fluxes between the HFIR and MITR reactors, there was a question of the impact of the rate of damage on irradiation swelling. The test samples were irradiated at relatively low temperatures and therefore recovery mechanisms should not be present. This assumption was verified as the MITR test samples, section 2.3.2, indicate similar irradiation swelling of approximately 0.7%, at similar damage level and test temperature.

2.3.2 Creep

The creep test coupons were stressed by bending at a constant radius with a surface strain of 0.025 and 0.05%. The samples were in contact with the coolant but there was no active flow, see Figure 2-13.

Figure 2-13 Creep test sample fixture. The samples are sandwiched between two curved plates that are tightly fitted into the rectangular holder.

Test sample profile was measured before and after irradiation with a laser micrometer. The profile of a sample loaded to a surface strain of 0.025% is shown in Figure 2-14. After 90 days of exposure (estimated ~0.7 dpa) the test sample showed no measurable permanent set and thus irradiation creep was insignificant. The profile length indicate a linear irradiation swelling of approximate 0.67%, consistent with the ORNL HFIR observation.

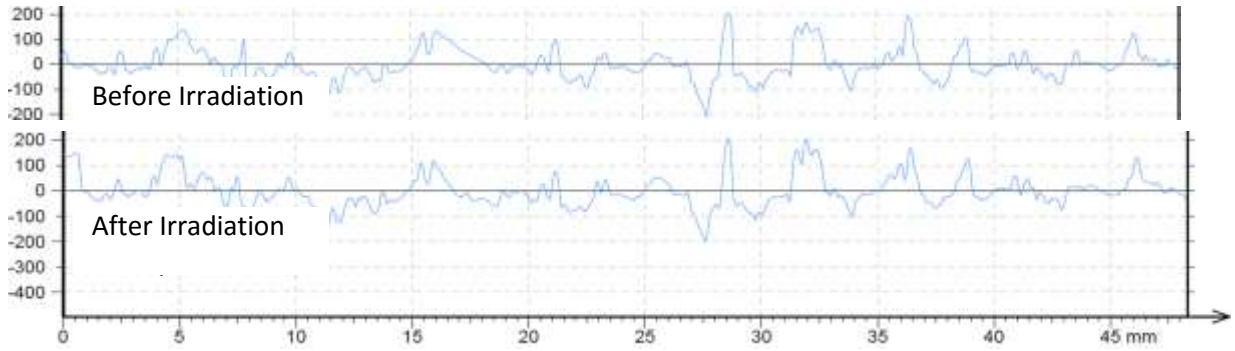

Figure 2-14 Test coupon profile before and after irradiation. No permanent set was observed.

2.3.3 Corrosion

Test sample weight loss after irradiation are tabulation in Table 2-8. Test samples located in the middle of the core experienced the greatest weight loss, up to 21.5%. The lower weight loss at the bottom and top of the core indicates the corrosion process is strongly neutron flux dependent. There was some variation in the creep coupon weight loss. Test samples stressed to 0.05% surface strain experienced an average weight loss of approximately 20%, less than the test samples stressed to 0.025% surface strain. There is no clear explanation except that the packing of the 0.05% strained samples may be tighter in some areas and thus slightly reduced flow.

Table 2-8 – Average sample weight loss by core location.

Core Location	Sample Type	Weight Loss (%)
Top	Flat coupon, corrosion	8.2
Middle	Flat coupon, creep	17.1
Bottom	Tube, corrosion	8.8

The high weight loss was a surprise since materials fabricated using the same CVD processing parameters tested in the same reactor under PWR conditions showed only minor weight loss. Post exposure photographs of a flat and tube coupons are shown in Figure 2-15. The flat channel coupon showed significant edge degradation while no apparent edge degradation is visible on the tube sample.

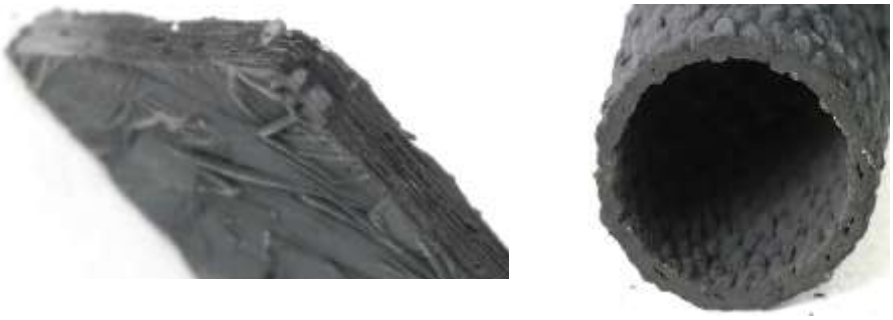

Figure 2-15 – Test samples after 90 days of exposure in the MIT research reactor.

Close up examinations of some of the surface fiber features on flat coupons indicate a diameter reduction of approximately 70 micrometer, Figure 2-16. Assuming a perfectly flat surface, a 35 micrometer material loss per side is equivalent to 4.4% sample mass loss. The surface area of the sample is significantly larger than a smooth surface and therefore direct CVD matrix material loss, assuming 50% more surface area would be more than 6.5% of the sample mass. This is still significantly lower than the measured mass loss of 17% for the flat coupon samples positioned in the middle of the core. A cross-sectional examination of the flat coupon showed significant subsurface attack, Figure 2-17.

Figure 2-16 – Surface fiber CVD coating diameter change.

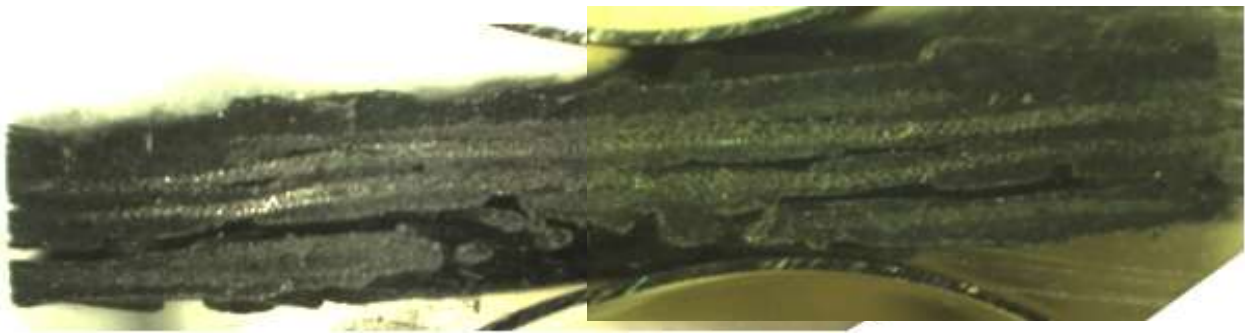

Figure 2-17 – Subsurface attack.

The oxidizing condition of the BWR-like coolant environment and fabrication processing variations were proposed as potential causes for the high mass loss. The theory of processing variation arose because higher corrosion resistance was observed for CVD material with large columnar microstructure, typical of higher temperature processing. However, potential performance change from microstructure improvement is limited and could not explain the orders of magnitude higher corrosion rate. To evaluate the higher oxidation potential of the BWR-like environment, a sister tube sample was inserted in a subsequent cycle with high hydrogen injection to simulate PWR conditions. After similar exposure time the tube sample showed no measureable mass change, Figure 2-18. Therefore, the observed high corrosion rate was likely caused by the oxidizing condition of the BWR-like coolant environment. Dissolved oxygen monitor showed several occurrences of oxygen excursions up to 1 ppm at the loop inlet and greater than 1 ppm at the loop outlet for the first two months of irradiation. Model calculations indicate the oxygen potential in the reactor would be even higher due to radiolysis. Higher corrosion rate was also observed in oxygenated autoclave test, thus supporting the oxygen potential theory. From a thermodynamic perspective, some oxidation of the SiC should be expected since it is not of the lowest energy state. It appears the oxidizing condition pushed the reaction over a threshold. Although the corrosion rate in PWR coolant chemistry was low, it may still pose a concern for PWR applications since hydrogen injection does not take place 100% of the time. The observed high corrosion rate in BWR environment is clearly not acceptable as it would lose structural integrity within the first cycle of operation.

Figure 2-18 – Tubing sample exposed to heavily hydrogenated PWR water chemistry. Measurement showed no weight loss.

2.3.4 Corrosion Mitigation

Oxidation is inevitable for a material not in the lowest thermodynamic energy state. For many of the engineering materials the corrosion/oxidation process creates a protective layer that dramatically slows down further oxidation. For SiC a corrosion product is SiO_2 and indeed a protective coating of silica had been observed in high temperature steam tests. Unfortunately SiO_2 has very high solubility in water and experimental evidence, both the MIT corrosion test and oxygenated autoclave tests, showed absence of a protective silica layer. It appears then

silica is dissolved as soon as it is formed and is not a rate controlling step in high temperature water environment.

The corrosion mitigation approach taken by this research effort is to stabilize the silica to form a protective layer. Since the main thrust of the current research effort is to characterizing the bulk properties of the SiC composite to enable the design of a functional BWR channel, it would render data already generated useless if the SiC matrix composition is modified. With this in mind, the research has been focused on surface modification. The idea is to fabricate SiC composite as before but near the end of the CVI/CVD process, add an additional precursor gas containing a stabilizing element. The number of silica compounds that are stable/insoluble in water is very limited. Amongst several candidates, zirconium silicate and titanium silicate were selected, primarily due to their formulae simplicity and existing interest in using them in nuclear applications. Several other silica containing compounds contained more elements and deemed too difficult to develop a suitable deposition technique.

2.3.4.1 ZrSiC Multi-components CVD Scoping Evaluation

The proposed surface modification requires multi-components CVD. Such capability did not exist and an initial scoping test was performed by an established commercial vendor using laboratory type of equipment. The desired coating components, Zr-Si-C, were deposited on the surface of smooth monolithic CVD blocks. The process produced a mixture of compositions across the surface as illustrated in Figure 2-19

. The coating parameters were proprietary to the vendor and are not available for reporting.

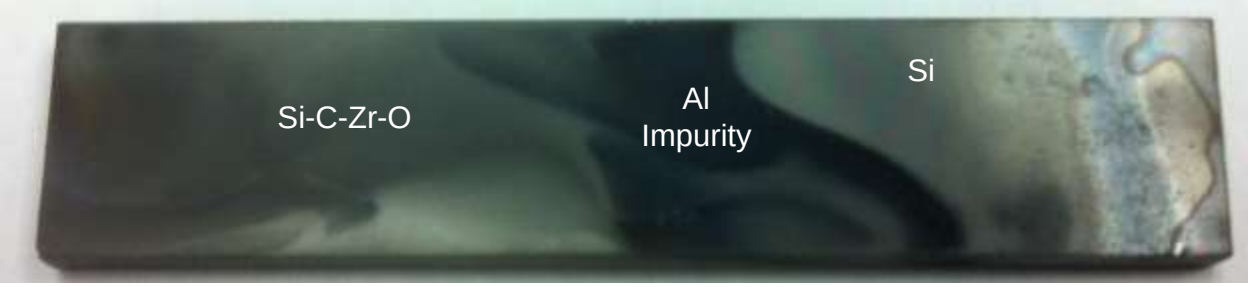

Figure 2-19 – ZrSiC deposition on CVD substrate.

The coated coupons were corrosion tested in 1 ppm oxygenated water autoclave. After 15 days of exposure portions of the coating totally oxidized and dissolved into the water but patches of what appears to be $ZrSiO_4$ remained, see Figure 2-20.

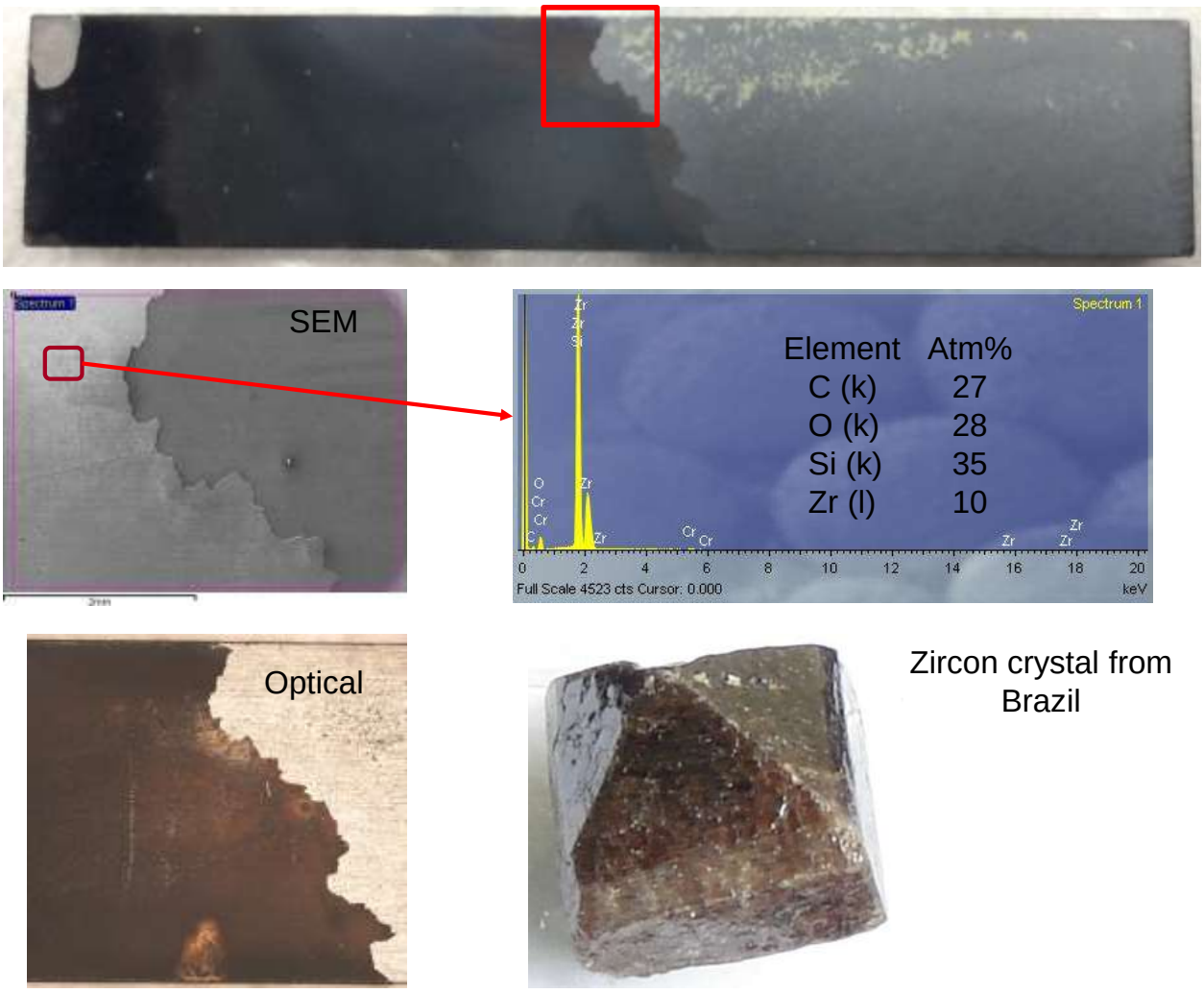

Figure 2-20 – Test coupon after 15 days exposure in 1 ppm oxygenated autoclave.

A second sample showed similar behavior after the corrosion test. Localized patches of the coating oxidized and likely dissolved into the water. It is likely these areas did not have the required chemical composition to form the more stable $ZrSiO_4$, as illustrated in Figure 2-19. A detailed examination of the sample, Figure 2-21 and Figure 2-22, showed the formation of a stable layer and has a chemical composition similar to $ZrSiO_4$.

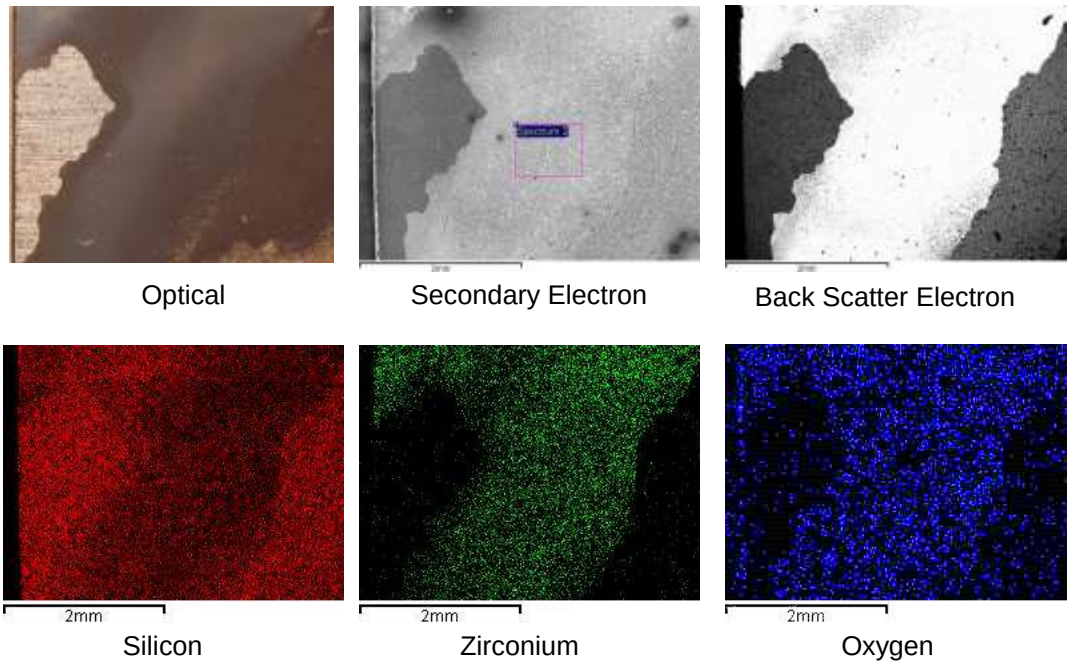

Figure 2-21 – Examination of a second sample showing local patches of what appears to be $ZrSiO_4$ composition.

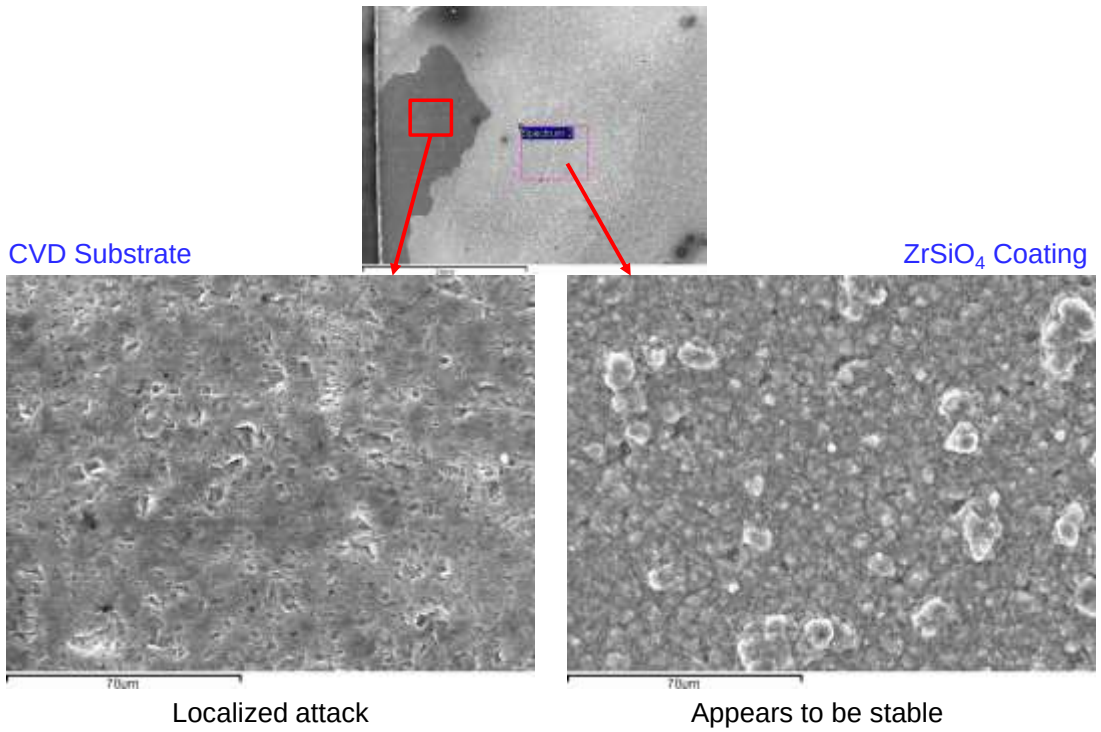

Figure 2-22 – Secondary electron image shows the formation of a stable layer, with composition similar to $ZrSiO_4$.

2.3.4.2 Additional Multi-component CVD Evaluation

The preliminary results based on the scoping test was encouraging, however, the vendor declined further development, likely due to lengthy development needed to establish a stable process.

Southwest Research Institute (SWRI) agreed to initiate a multi-component CVD process development using existing equipment. A schematic of the apparatus is shown in Figure 2-23. The system is composed of a tube furnace with fittings for various precursor gas input and vacuum pumps. A long quartz tube is used as the reaction chamber. Since the precursor gas is a solid at room temperature, a bubbler is employed to vaporize the source material.

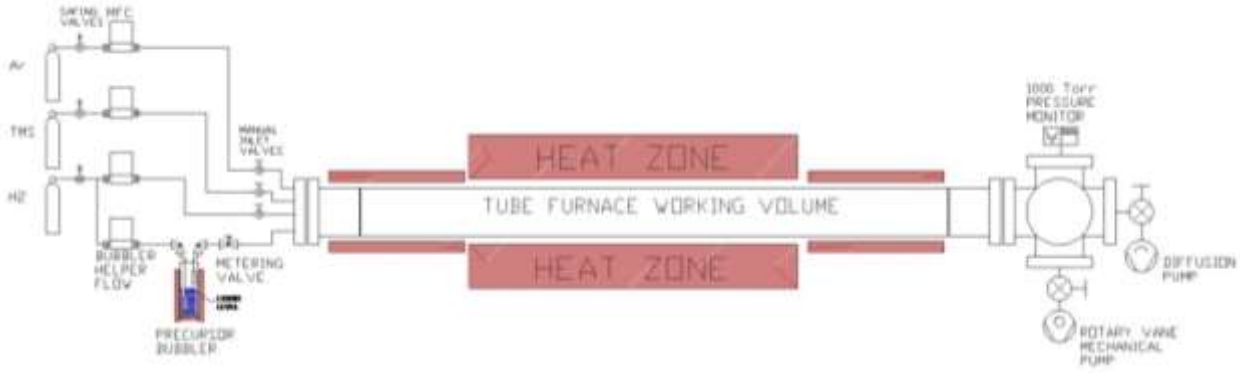

Figure 2-23 – Multi-components CVD apparatus layout.

Precursor gas for the formation of SiC was trimethylsilane. Hydrogen gas was used as a carrier gas and to control the thermodynamic conditions within the reaction chamber to facilitate SiC formation. $TiCl_4$ or $ZrCl_4$ were precursor gases for the deposition of TiC or ZrC, respectively. The flow rates of Ar, H_2 and TMS gases were precisely controlled and measured. However, the flow rates of titanium or zirconium chlorides could not be precisely controlled or measured. Deposition was conducted at 1100°C. Precursor feed rates were adjusted trial by error to target the desired composition of 1:1 Ti/Zr:Si atomic ratio. The desired composition was achieved with TiSiC but not with ZrSiC. The deposition of ZrC is more favorable at higher temperatures relative to SiC. Representative photographs of test coupons are shown in Figure 2-24. Coating details and sample characterization were provided in reference 10.

(a) (b)

Figure 2-24 Representative coated samples, (a) TiSiC 1:1 Ti:Si ratio and (b) Zr doped SiC with 2-5% atomic Zr content.

The coated coupons were corrosion tested in a refreshed and oxygenated autoclave [11]. The dissolved oxygen concentration in the water was controlled at 1 ppm. Test samples were weighted at 7, 14 and 28 days of exposure. A few samples showed a rate change after 7 days of exposure but the rate did not continue to decrease after 14 days, indicating the failure to form a protective layer. After 28 days of exposure the test samples were examined in detail.

TiSiC

Visual examination of the test samples confirmed the weight measurements. The coating on most of the samples had corroded away. One of the coupons had a local patch of Ti_2SiC composition also corroded away. Minor residue still remain on some of the samples and an example is shown in Figure 2-25. X-ray analysis of the residue indicates the presence of some titanium but it is far from the $TiSiO_4$ composition. High magnification image of the residue indicate a corrosion product of Ti-Si-O was formed, but it appears to be porous and not stable.

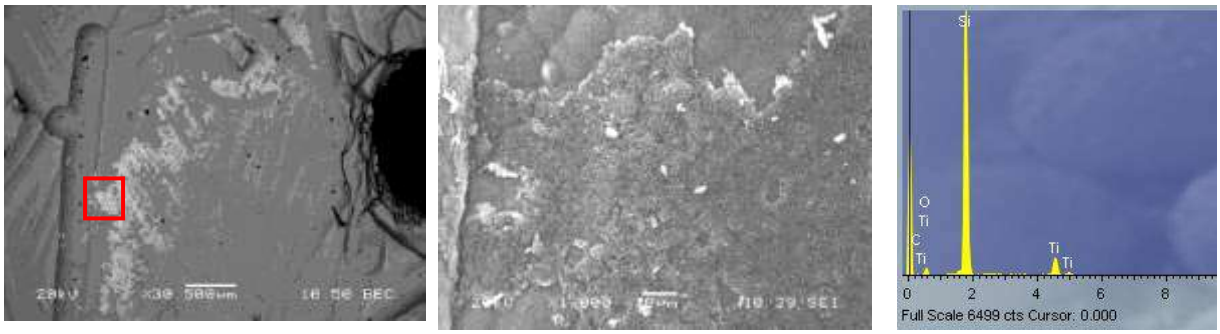

(a) (b) (c)

Figure 2-25 – Secondary electron images of a local patch of corrosion residue (a) low magnification of residue, (b) high magnification image of the region enclosed by red box, and (c) X-ray emission from the patch.

Zirconium Doped Sample

The zirconium doped samples were similarly examined after 28 days of autoclave exposure. As is in the case of the titanium doped samples, most of the coating had corroded away but local patches of material remained. Examples of localized patches are shown in Figure 2-26. X-ray spot analyses of several patches showed compositions expected of $ZrSiO_4$. Unlike the titanium doped residue, the zirconium doped patches appears to be non-porous and continuous. As the coated samples only contained 2-5% zirconium, additional research is needed to determine if a protective continuous $ZrSiO_4$ layer could be form if more zirconium is present in the coating.

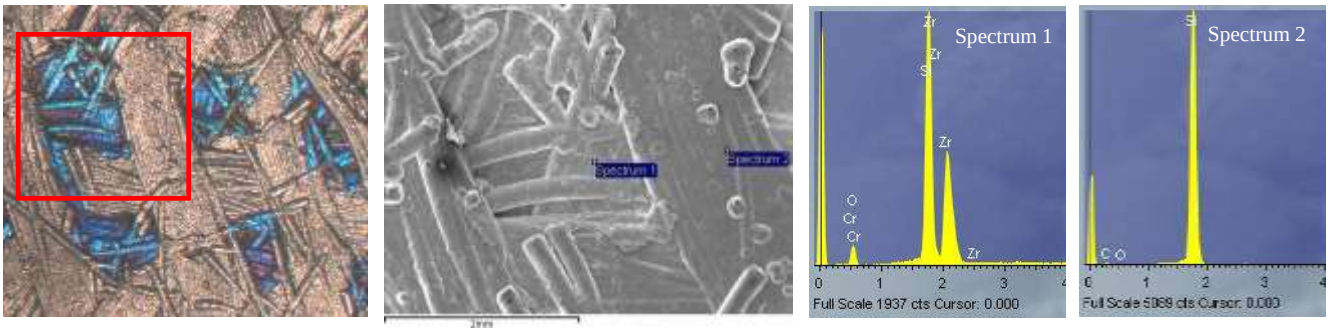

(a) (b) (c)

Figure 2-26 Detailed examination of zirconium doped sample, (a) Optical image of local patches, (b) secondary electron image of the patch enclosed by the red rectangle, and (c) X-ray spot analyses.

2.3.4.3 Multi-components CVD Equipment Upgrade

Literature data suggests the composition of ZrC deposition changes with temperature [8]. Taking advantage of a system upgrade, additional coatings were attempted at temperatures higher than 1100°C. Unfortunately, this effort did not produce good samples and the effort was terminated.

3 SUMMARY AND CONCLUSIONS

An extensive evaluation was performed to determine the suitability of using SiC composite as a BWR channel material. An initial feasibility evaluation identified fragmentation resistance and differential irradiation induced volumetric swelling as key obstacles to the realization of the concept. Both of these issues were addressed through analysis and experimentation. Test data generated in this project indicate SiC composite could meet the mechanical design requirement of a BWR channel. However, the material exhibited high corrosion (oxidation) rate under BWR oxidizing conditions. In order to implement the SiC based channel concept the high corrosion rate must be mitigated.

Evaluations/testing conducted thus far could be summarized as follow:

1. SiC composite with the proper fiber geometry is resistant to fragmentation even when punctured.
2. Irradiation induced volumetric swelling may cause a temporary channel bow due to fast neutron flux gradient. The condition is acceptable up to 25% flux gradient.
3. Mechanical strength is significantly lower relative the existing zirconium based channels. Under limiting seismic conditions portions of the wall thickness around corners may exceed the proportional limit. However, it is believed the strength could be improved with higher fiber content. Exceeding the proportional limit under seismic condition may be acceptable since stress is very low at operating condition and micro-cracks are not expected to propagate.
4. Irradiation at prototypical BWR operating temperatures verified volumetric swelling at saturation is approximately 2% at 1 displace per atom damage level.
5. Creep was not detected during the 2.5 effective full power month of irradiation. Therefore the channel is not expected to bow or bulge.
6. SiC offers exceptionally oxidation resistance at high temperatures up to 1600°C under limited steam flow conditions. Published test results indicate the mass loss may be steam flow rate dependent.
7. Full SiC composite channel cross-section is resistant to thermal shock when quenched from LOCA temperatures in cool water
8. Significant corrosion/oxidation was measured under BWR oxidizing coolant conditions. Up to 20% mass loss was detected after 2.5 months of irradiation.
9. The high corrosion rate must be mitigated for the concept to be viable. Corrosion product stabilization by the addition of zirconium into the CVD process is promising, but a viable deposition process need be developed to verify its functionality.

4
REFERENCES

1. Katoh, Y., Ozawa, K., Hinoki, T., Choi, Y., Snead, L.L., Hasegawa, A., "Mechanical Properties of Advanced SiC Fiber Composites Irradiated at Very High Temperatures", Journal of Nuclear Materials, 417 (2011), 416-420.
2. Katoh, Y. and Snead L., "Operating Temperature Window for SiC Ceramic and Composites for Fusion Energy Applications", Fusion Science and Technology, Vol 56, Aug. 2009.
3. Katoh, Y. and Kohyama, A., "Progress in SiC-Based Ceramic Composites for Fusion Applications", Fusion Science and Technology, Vol 44, Jul 2003.
4. Feinroth, H., Ales, M., Barringer, E., Kohse, G., Carpenter, D. & Jaramillo, R. "Mechanical Strength of CTP Triplex SiC Fuel Clad Tubes After Irradiation in MIT Research Reactor under PWR Coolant Conditions" The 33rd International Conference on Advanced Ceramics & Composites, 2009
5. Yueh, K., et al., "Clad in clay", Nuclear Engineering International, March 08, 2010.
6. Feinroth, H., "Silicon Carbide TRIPLEXTM Fuel Clad for Accident Resistance and Durability", 1st ICMST Conference, 2012 Japan Society of Maintenology, 2012
7. Yueh, K. and K. Terrani, "Silicon carbide composite for light water reactor fuel assembly applications", JNM, Vol 448, Issues 1-3, May 2014.
8. Wang, Y., Liu, Q., Liu, J., Zhang, L. and Cheng, L., "Deposition Mechanisms for Chemical Vapor Deposition of Zirconium Carbide Coatings", J. Am. Ceram. Soc. 91(4)1249-1252, 2008.
9. F. Franceschini, E.J. Lahoda, "Neutronic Behavior and Impact on Fuel Cycle Cost of Silicon Carbide Clad," 2010 ANS Winter Meeting, Las Vegas, NV, 2010.
10. Deliverable M3CA-12-CA-EPRI-0402-099, "SiC Surface Treatment/Coating Process Development", April 22, 2016
11. Deliverable M3CA-12-CA-EPRI-0402-0910, "Autoclave Corrosion Testing of Surface Treated Samples", September 20, 2016